# Designing Natural Formations of Low Earth Orbitting Satellites

Phil Palmer & Mark Halsall

January 25, 2013

Surrey Space Centre,
University of Surrey
Guildford GU2 7XH
England.

**Abstract**

In this paper we describe possible natural formations for satellites in low Earth orbit which exploit the Earth's oblateness. These formations are based upon an analytic model of natural formations for satellites in nearly circular orbits, which has already been published, and explores the range of formations available. We describe how we parameterise the formations and then derive from this parameterisation the orbital elements needed for each satellite orbit and then show the long term evolution of these orbits to show the slow evolution of the formation geometry over time. We demonstrate the formations maintain their projected shape in the sky without control over a day, in the presence of gravitational perturbations. This shows that the control requirements for long term maintenance of such formations can be reduced considerably for long term maintenance.

Correspondence to:
Phil Palmer,
Surrey Space Centre,
University of Surrey,
Guildford GU2 7XH,
UK.
Tel: +44 1483 686024.
Fax: +44 1483 689503.
Email: P.Palmer@surrey.ac.uk

# Nomenclature

| | | |
|---|---|---|
| $\varpi, \upsilon, \zeta$ | = | curvilinear coordinates on sky with $\varpi$ measuring depth |
| $\varpi_F, \upsilon_F, \zeta_F$ | = | solid body component to motion of formation |
| $\varpi_S, \upsilon_S, \zeta_S$ | = | internal component to motion of formation |
| $\varpi_M, \upsilon_M, \zeta_M$ | = | maximum variation in curvilinear coordinate by formation |
| $\varpi_0, \upsilon_0$ | = | centre about which satellite oscillates in curvilinear coordinates |
| $\phi_\varpi, \phi_\upsilon, \phi_\zeta$ | = | phases of oscillation in each curvilinear coordinate |
| $I$ | = | inclination of guiding centre motion |
| $a$ | = | semi-major axis of guiding centre motion |
| $\widehat{a}_k, \widehat{I}_{k0}, \widehat{\Omega}_{k0}$ | = | differences in epicycle elements of satellite $k$ and guiding centre |
| $\theta, \kappa$ | = | secular variations included in guiding centre motion |
| $\chi$ | = | long periodic variation evaluated for guiding centre orbit parameters |
| $R$ | = | equatorial radius of Earth |
| $\tau$ | = | phase along guiding centre orbit |
| $\alpha_e, \alpha_{Pk}$ | = | phase shift for equator crossing and perigee for satellite $k$ |
| $e_k$ | = | eccentricity of orbit for satellite $k$ |

# 1 Introduction

Many planned missions are now beginning to take advantage of the benefits offered by the use of satellite formations. In addition to the generally lower cost associated with development and launch of smaller satellites, reduced risk of a mission-ending critical failure, and greater flexibility offered by the ability to reconfigure the formation, missions are being planned which can only be achieved by the use of multiple spacecraft. Amongst other objectives, the GRACE mission [1] uses a pair of satellites flying in formation in Low Earth Orbit (LEO) to make accurate gravitational measurements. Formation flight for a string-of-pearls formation has been demonstrated by the Space Technology 5 (ST5) mission [2, 3]. Increasing the complexity of the formation design from linear configurations, the Auroral Lites mission [4] uses four satellites in a tetrahedral pattern. The TanDEM-X [5] mission will fly in close formation with the already-launched TerraSAR-X satellite to provide elevation measurements of the Earth's surface. TerraSAR-X is one of several missions proposed that use formation flying satellites for Synthetic Aperture Radar (SAR) [6, 7]. In an extension to the SAR technique, Zink [8] et al consider an interferometric cartwheel using three satellites in formation to maintain a near uniform radial baseline.

Much work on formation design has adopted the Hill-Clohessy-Wiltshire Eqs. [9] used to model the approach to rendezvous and docking. This may be considered the limit of the epicycle model [10] when the geopotential is Keplerian. The advantage of using these equations is that they have a particularly simple form, and the out-of-plane motion decouples from the other directions. Sabol et al [11] present a technique for designing satellite formations in this frame and use it to design a set of formations that are geometrically simple. They show how to determine initial conditions for each satellite to produce the formations. Among the formations they present is the projected circle formation. This paper is a natural extension of this work to other projected formations that exploit the Earth's oblateness.

In this paper we focus upon the design of satellite formations in low Earth orbit, exploiting the natural dynamics, to remove the need for station-keeping against the principal disturbing effects of earth oblateness. The aim of the design process is to determines a set of orbital parameters for each of the satellites, so that the natural dynamics will approximately maintain a formation geometry under $J_2$ and $J_3$ terms. Higher-order terms are then treated as a disturbance to the formation, which require a much smaller control thrust to correct for. Such formations are of interest for observing the Earth and its environment. As a consequence, we shall pay particular attention to the projected geometries of the formation onto the plane of the sky. We assume that the satellites move on nearly circular orbits in order to remove the shearing effect experienced in more eccentric orbits. Lane and Axelrad [12] have considered formation design for elliptic orbits. Their method uses orbital element differences in a similar way to this work, but is based on unperturbed Keplerian orbits.

Once the effects of earth oblateness are incorporated, the problem of establishing formations and inverting the equations to find orbital parameters is more difficult. Guibout and Scheeres [13] present the problem of formation design, when $J_3$ is incorporated into the dynamics, as a boundary-value problem. Their approach aims to bring the satellites into a given configuration at a given time, rather than being in a given configuration over an extended period. This approach is therefore very different from the approach we adopt here.

# 2 Relative Epicycle Model

This paper uses the relative orbit model presented by the authors in [14, 15], a relative motion model based on the epicycle orbit model developed by Hashida and Palmer [10, 16]. The epicycle model describes orbits with small eccentricity and can incorporate all the geopotential terms and atmospheric drag. The position and velocity of the satellite is described using four coordinates to define the orbital plane and position,

and two components of velocity on the orbital plane. The four spatial coordinates $(r_k, \lambda_k, I_k, \Omega_k)$ define the satellite position in an inertial frame. These are shown in Fig. 1. Associated with these coordinates is a set of orbital elements, or epicycle elements. These are defined as $\mathbf{x}_E = (a, e, I_0, \Omega_0, \alpha_P, \alpha_e)$. Here $a$ and $e$ are the orbital semi-major axis and eccentricity, $I_0$ and $\Omega_0$ define the orbital plane at the instant of equator crossing at the chosen origin of time (Note that the inclination and RAAN will vary periodically and secularly over time); $\alpha_P$ and $\alpha_e$ are the epicycle phases at perigee passage and equator crossing. For a single satellite we can choose the origin of time at equator crossing and set $\alpha_e = 0$. This is not, however, possible when considering a formation of satellites crossing the equator at different times.

The motion of a single satellite in the epicycle model, moving under the effects of $J_2$ and $J_3$ is given by:

$$\begin{aligned} r &= a(1+\rho) - ae\cos(\tau - \alpha_P) + a\chi\sin\tau + \Delta_r\cos 2\tau \\ \lambda &= \tau(1+\kappa) + 2e\left[\sin(\tau-\alpha_P) - \sin\alpha_P\right] - 2\chi[1-\cos\tau] + \Delta_\lambda\sin 2\tau \\ I &= I_0 + \Delta_I(1-\cos 2\tau) \\ \Omega &= \Omega_0 + \theta\tau + \Delta_\Omega\sin 2\tau \\ \tau &= nt \end{aligned} \tag{1}$$

where the secular variation due to $J_2$ is described by the terms $\theta$ and $\kappa$, the long periodic effects of $J_3$ are given by $\chi$ and the short-periodic effects by $\Delta_i$.

The description of relative motion using these epicycle coordinates is defined with respect to a guiding centre that moves on a circular orbit which secularly drifts due to the effects of $J_2$ on a satellite orbit. As there are no periodic terms involved in the motion of this guiding centre, then no satellite can be placed on the origin and remain there over time. This choice is convenient as it removes the principle secular effect on the formation, while leaving in all the periodic motions of the satellites. The position of the guiding centre is also shown in Fig. 1 where a subscript $c$ is used to denote the co-ordinates defining its instantaneous orbital plane. The motion of each satellite in the formation can then be described relative to this guiding centre by a set of epicycle elements $\mathbf{x}_k = (\hat{a}_k, e_k, \hat{I}_{k0}, \hat{\Omega}_{k0}, \alpha_{Pk}, \alpha_e)$ where $k$ denotes the satellite in the formation.

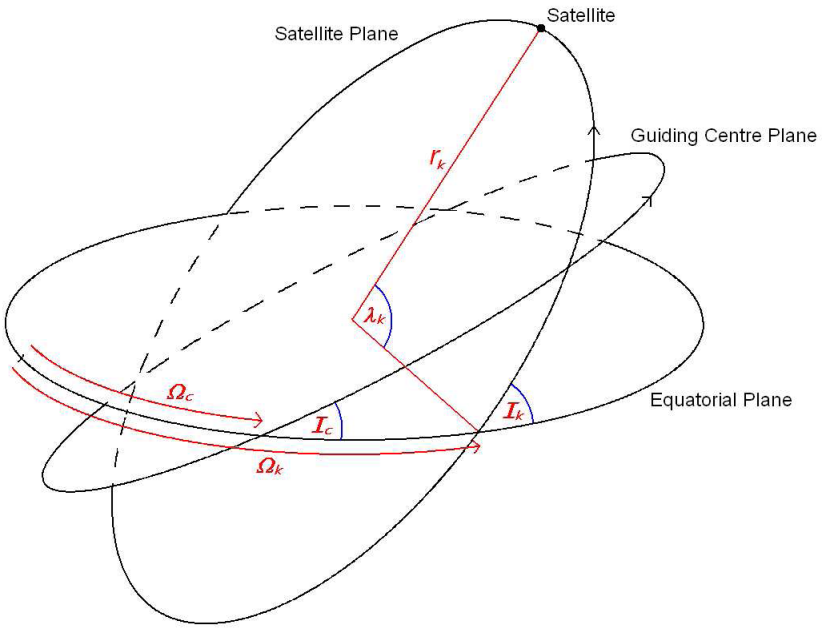


Figure 1: Epicycle Coordinates of one satellite and the guiding centre motion plane.

The caret denotes epicycle elements relative to the guiding centre. There are relative secular drifts between these satellites and the guiding centre, caused by $J_2$. As shown in [15], these differential drifts can be removed by adjusting the semi-major axes $\hat{a}_k$. Knowing the motion of the guiding centre and these epicycle elements is enough to completely determine the motion of the satellite in inertial space.

The description of the relative motion described in Ref. [15] uses a curvilinear coordinate system $(\varpi, \upsilon, \zeta)$ where $\varpi$ denotes the difference in radial distance of the satellite and guiding centre, and $(\upsilon, \zeta)$ are defined on the celestial sphere as shown in Fig. 2. This system is similar to that used in modelling proximity operations for the shuttle [17]. More details of the definitions of these coordinates and the motion of the satellite relative to the guiding centre can be found in [15]. Since the guiding centre moves on a perfectly circular orbit and we can fix our origin of time when this origin crosses the equator at an ascending node, then we need only three epicycle elements to define the motion of the guiding centre: $\mathbf{x}_c = (a, I, \Omega_{c0})$. Note that $\Omega_c$ drifts secularly in time, hence we use the instantaneous RAAN initially, but inclination is constant in

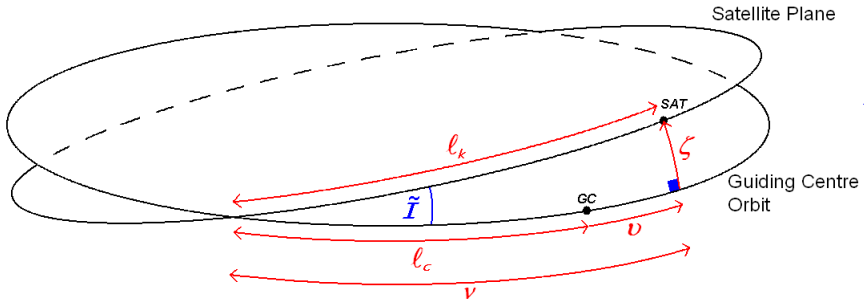


Figure 2: Curvilinear Coordinates for Relative Satellite Positions.

time. The epicycle phase $\alpha$ defines where along this orbit the guiding centre is at any particular time, where $\tau = nt$ and $n$ is the mean motion associated with the guiding centre orbit.

The dynamical model for the motion of each satellite in the formation can be split into two separate parts: one that is common to all satellites in the formation (the solid body motion) and a second that varies from satellite to satellite (the internal motions) [15]. The first part can be described by the expressions:

$$\varpi_F = -a\chi \sin\tau + \frac{1}{4} J_2 \left(\frac{R}{a}\right)^2 a \sin^2 I \cos 2\tau \tag{2}$$

$$\upsilon_F = 2\chi(\cos\tau - 1) + \frac{1}{8} J_2 \left(\frac{R}{a}\right)^2 \sin^2 I \sin 2\tau \tag{3}$$

and

$$\zeta_F = -\frac{3}{4} J_2 \left(\frac{R}{a}\right)^2 \sin 2I \sin\tau \tag{4}$$

where $\chi$ denotes the long periodic effects of $J_3$ and $R$ is the equatorial radius of the Earth. We consider the motion to be principally periodic with the orbital period, and treat the terms at twice this frequency as smaller. This is reasonable for most inclinations. This describes the periodic way the formation moves around the guiding centre, but it does so as a rigid configuration which does not distort. The other part

of the motion describes the individual relative motions of satellites in the formation, and so describes the changes in the formation geometry:

$$\varpi_S = \widehat{a}_k - \theta a \sin I \widehat{I}_{k0} - a e_k \cos\left[(1-\kappa)\tau - \alpha_{Pk}\right] \tag{5}$$

$$\upsilon_S = -\alpha_e(1+\kappa) + 2e_k \sin(\alpha_{Pk} - \alpha_e) + \widehat{\Omega}_{k0} \cos I - \frac{1}{2}\widehat{I}_{k0}\widehat{\Omega}_{k0} \sin I + 2e_k \sin\left[(1-\kappa)\tau - \alpha_{Pk}\right] \tag{6}$$

$$\zeta_S = \widehat{I}_{k0} \sec\Phi \sin\left[\tau - \Phi\right] \tag{7}$$

where

$$\tan\Phi = \sin I \left(\widehat{\Omega}_{k0} + \widehat{\theta}_k \tau\right) / \widehat{I}_{k0} \tag{8}$$

The combination of these two components of the motion give a complete description of the satellites with respect to the guiding centre, to the level of accuracy employed. Depending upon the application, we may not worry too much how the formation of satellites moves in the sky as long as the geometric configuration is maintained. In this case we need only consider the second part of this motion described by Eqs. (5) - (8). For other applications we may wish to keep the projected formation on the sky moving along a regular path, in which case we need to include both parts of the motion.

With this in mind we note that Eqs. (5) - (8) can be written in the form:

$$\varpi = \varpi_0 + \varpi_M \cos(\tau + \phi_\varpi) \tag{9}$$

$$\upsilon = \upsilon_0 + \upsilon_M \sin(\tau + \phi_\upsilon) \tag{10}$$

$$\zeta = \zeta_M \sin(\tau + \phi_\zeta) \tag{11}$$

where

$$\varpi_0 = \widehat{a}_k - \theta a \sin I \widehat{I}_{k0} \qquad \varpi_M = -a e_k \qquad \phi_\varpi = -\alpha_{Pk} - \kappa\tau \tag{12}$$

$$\upsilon_0 = -\alpha_e(1+\kappa) + 2e_k \sin(\alpha_{Pk} - \alpha_e) + \widehat{\Omega}_{k0} \cos I - \frac{1}{2}\widehat{I}_{k0}\widehat{\Omega}_{k0} \sin I \tag{13}$$

$$\upsilon_M = 2e_k \qquad \phi_\upsilon = -\alpha_{Pk} - \kappa\tau \tag{14}$$

and

$$\zeta_M = \widehat{I}_{k0} \sec \Phi \qquad \phi_\zeta = -\Phi \tag{15}$$

When we combine both parts of the motion then we can still describe the motion in terms of (9) - (11) where now:

$$\varpi_0 = \widehat{a}_k - \theta a \sin I \widehat{I}_{k0} + \frac{1}{4} J_2 \left(\frac{R}{a}\right)^2 a \sin^2 I \cos 2\tau \tag{16}$$

$$\varpi_M = a\sqrt{e_k^2 + \chi^2 + 2\chi e_k \cos(\alpha_{Pk} + \kappa\tau)} \tag{17}$$

$$\tan \phi_\varpi = -\frac{e_k \sin(\alpha_{Pk} + \kappa\tau)}{\chi + e_k \cos(\alpha_{Pk} + \kappa\tau)} \tag{18}$$

and

$$\upsilon_0 = -\alpha_e(1+\kappa) + 2e_k \sin(\alpha_{Pk} - \alpha_e) + \widehat{\Omega}_{k0} \cos I - \frac{1}{2}\widehat{I}_{k0}\widehat{\Omega}_{k0} \sin I - 2\chi + \frac{1}{8} J_2 \left(\frac{R}{a}\right)^2 \sin^2 I \sin 2\tau \tag{19}$$

$$\upsilon_M = 2\sqrt{e_k^2 + \chi^2 + 2\chi e_k \sin(\alpha_{Pk} + \kappa\tau)} \tag{20}$$

$$\tan \phi_\upsilon = \frac{\chi - e_k \sin(\alpha_{Pk} + \kappa\tau)}{e_k \cos(\alpha_{Pk} + \kappa\tau)} \tag{21}$$

and

$$\zeta_M^2 = \left(\widehat{I}_{k0} - \frac{3}{4} J_2 \left(\frac{R}{a}\right)^2 \sin 2I\right)^2 + \sin^2 I \left(\widehat{\Omega}_{k0} + \widehat{\theta}_k \tau\right)^2 \tag{22}$$

$$\tan \phi_\zeta = -\frac{\sin I \left(\widehat{\Omega}_{k0} + \widehat{\theta}_k \tau\right)}{\widehat{I}_{k0} - \frac{3}{4} J_2 \left(\frac{R}{a}\right)^2 \sin 2I} \tag{23}$$

These results show that in both cases the motion can be described by the same equations, although the relationships between the above parameters and the orbital elements depends upon whether the whole motion is incorporated.

# 3 Design Parameters

The expressions for the relative motion can be described through the simple relations (9)- (11). If we consider the projection of this 3D motion in the planes of any two of the local coordinates, then we obtain an ellipse. In particular, we are most interested in the projection of the motion onto the plane of the sky, which is the $(\upsilon, \zeta)$ plane. We may exploit this simple geometric description to design formations of satellites with varying applications. In this section we will define a set of design parameters which we have found useful in capturing the types of relative motion that may be exploited for differing formation designs.

The lack of any constant term in equation (11) means that the elliptic projection of the relative motion on the plane of the sky has its centre along the $\upsilon$ axis. There is only one parameter required to determine where along this axis the centre of the ellipse will be. We call this parameter $c$. This determines the distance from the centre of the relative motion of one satellite with respect to the guiding centre. Since the guiding centre is a virtual reference point, we have the freedom to move it so that $c = 0$. When there are multiple satellites moving along different projected ellipses, then each ellipse will have a different value of c associated with it.

We may define two ellipse parameters for the semi-major and semi-minor axes, $a$ and $b$, and the orientation of the ellipse with respect to the $\upsilon$ axis, $\sigma$. Here $(0 < \sigma < \pi)$. We require two further parameters, the first is $\varphi$, which determines the initial phase around the ellipse to place the satellite, and the second $d$, determines which way around the projected ellipse the satellite will appear to move. This last parameter takes the values of $\pm 1$ where $+1$ implies motion appears clockwise on the sky, and $-1$ anti-clockwise.

We illustrate this set of design parameters in Fig. 3, where we show the projected ellipse as it would appear in the plane of the sky.

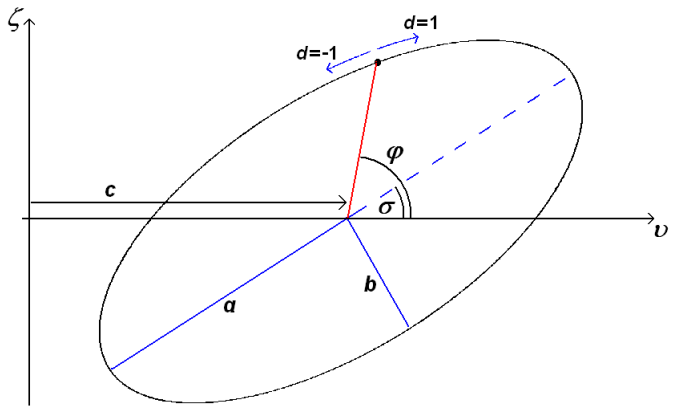


Figure 3: Ellipse design parameters describing the relative motion of a satellite as seen in the plane of the sky.

# 4 Possible Configurations

We may now consider the design of formations of satellites based upon these design parameters and in the following section we shall review some of the formations that may be constructed using the natural control-free dynamics of LEO satellites. There is considerable flexibility in the choice of design parameters, so we shall indicate only the nature of some of the more useful types of formations that can be created.

## 4.1 Leader-Follower

The simplest formation design is for a pair of satellites with one satellite following another along the same orbit. This would be equivalent to both satellites being on the same projected ellipse, so that only the parameter $\varphi$ is different. In this case we can fix $c = 0$ by a suitable choice of guiding centre. The baseline between the satellites varies as they move around the ellipse, and the maximum variation is obtained by separating them in phase by $\pi$. The baseline varies unless $a = b$, and the orientation varies according to $\sigma$.

Alternatively, the two satellites may be placed on separate projected ellipses, which allows for considerable variation in baseline length and orientation in the sky. If these two ellipses have $b = 0$ and $\sigma = 0$ then the baseline will be fixed in the $\upsilon$ direction and

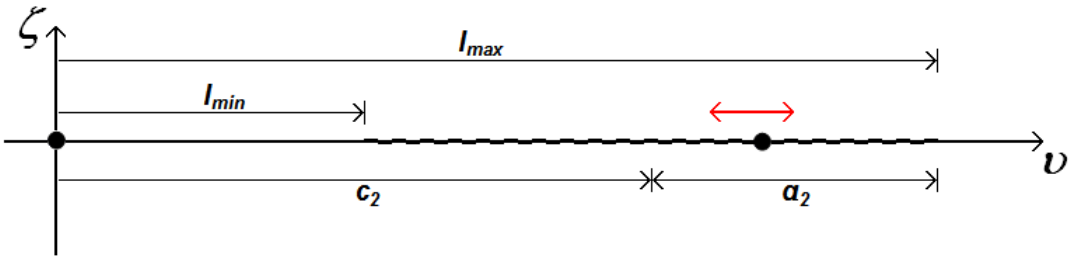


Figure 4: Along-track linear formation

grow and shrink. In such a scenario, we may place one satellite on the guiding centre and choose the parameters for the second satellite according to:

$$a_2 = \frac{1}{2}\left(\ell_{max} - \ell_{min}\right) \tag{24}$$

$$c_2 = \frac{1}{2}\left(\ell_{max} + \ell_{min}\right) \tag{25}$$

The separation between these satellites now oscillates between $\ell_{max}$ and $\ell_{min}$, as shown in Fig. 4.

**Fixed Rotating Configurations** If we fix $a = b$ then the projected ellipse becomes a circle. Satellites move around such circles at constant angular rates, with period equal to the orbital period. If we select satellites to move on such projected circles, with the same centre then we can choose $c = 0$ and for a circle $\sigma$ has no meaning so may be set it to zero also. The satellites move in the same direction, so $d$ is fixed for all of them. By changing the phase $\varphi$ and radius $a$ of the projected circles we can create regular patterns such as that described in Fig. 5. As the satellites move around the projected circles, the grid will rotate as a fixed pattern in the sky. Other more imaginative patterns can be created such as shown in Fig. 6.

**Pulsating Configurations** It is possible to combine the geometry of the fixed configurations with the dynamic baseline of the leader-follower pair. To do this we

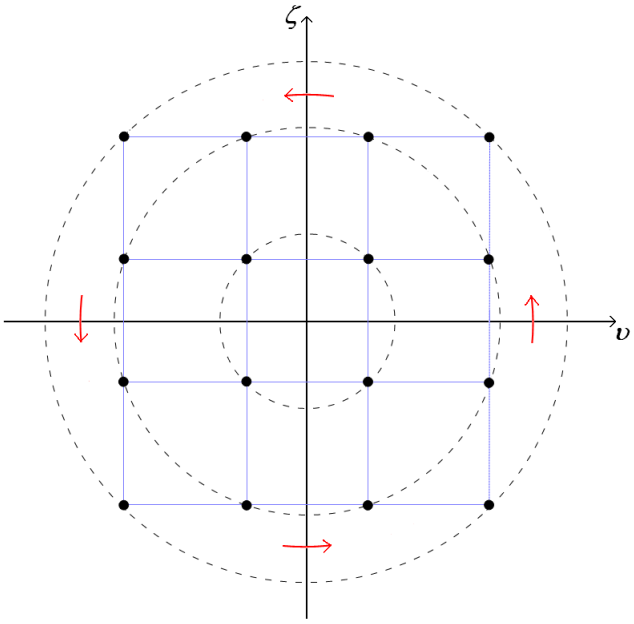


Figure 5: Rotating grid formation. Dashed lines show the projected circles that the satellites appear to move around in the sky.

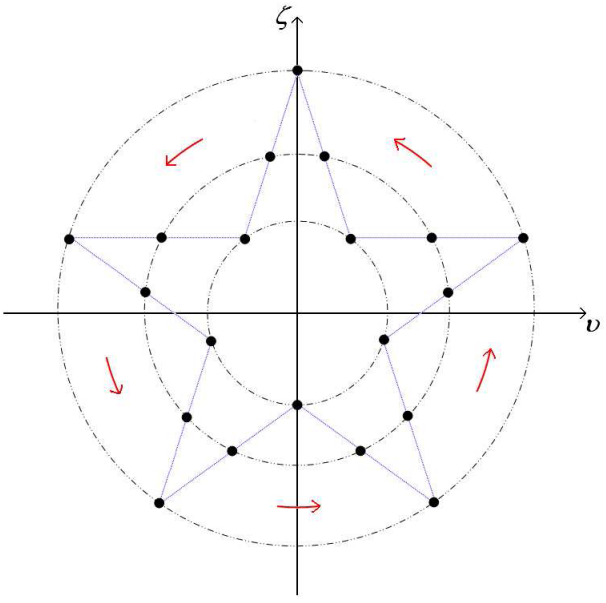


Figure 6: This five-pointed star formation. Dashed lines show the projected circles that the satellites appear to move around in the sky.

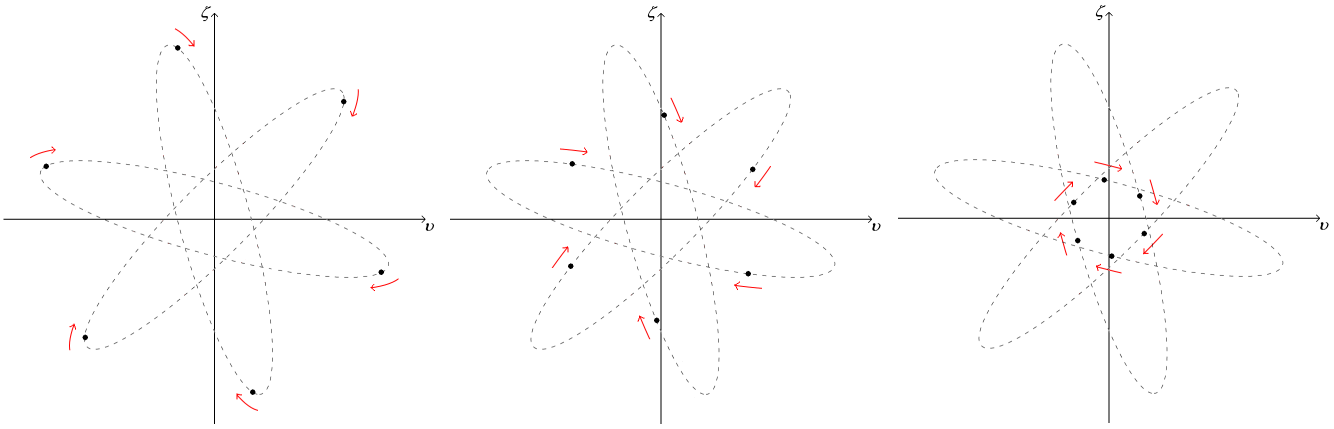


Figure 7: Monodirectional varying radius projected circle formation

place satellites on projected ellipses which all have the same shape and centre, but are rotated on the plane of the sky. In this case we can again choose $c = 0$ and fix $a$, $b$ and $d$ for all the satellites. The values of $\sigma$ and $\varphi$ are chosen so that satellites sit in some geometric configuration, such as the circle shown in Fig. 7. In this example we have chosen to distribute the ellipses in constant intervals in $\sigma$ and placed two satellites on each projected ellipse. The angles $\varphi$ are determined by the condition of being on the projected circle. As the satellites move around the projected ellipses, the circle diminishes in radius until reaching a minimum and then increases back to a maximum. The formation therefore pulsates in the sky.

If we allow satellites to move in the opposite sense around the projected ellipses, then we can increase the number of satellites per ellipse to four. The satellites do not collide due to differences in the radial distance from Earth to maintain the formation. Such a configuration is shown in figure (8).

These formations exploit the symmetry by creating the same baseline lengths between corresponding pairs of satellites in the two ellipses, oriented differently on the sky. The effect is to make the baselines diameters of a pulsating circle on the sky. These baselines can be varied if we do not distribute the values of $\sigma$ uniformly. The satellites still remain on the projected circles, but the baselines are more varied.

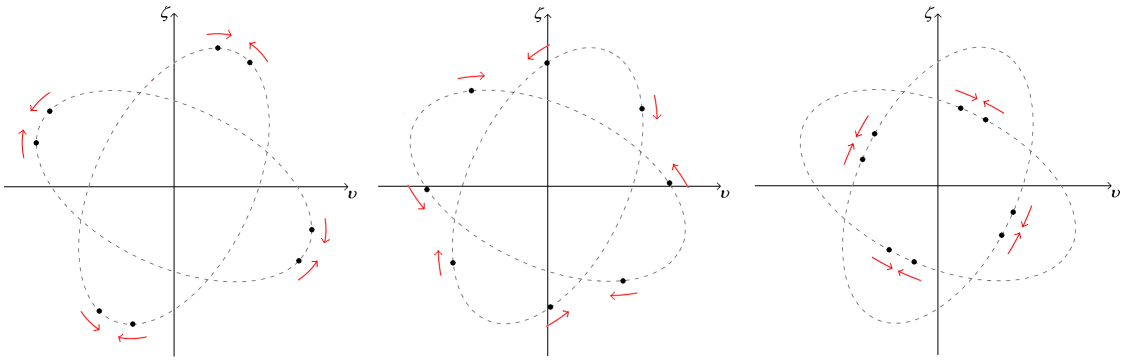


Figure 8: Bidirectional varying radius projected circle formation

# 5 Determination of Required Orbital Elements

We now consider the problem of determining the orbital elements we require to generate the set of design parameter values we need to realise these formations. We break this into three stages: firstly to relate the design parameters $\mathbf{x}_D = (a, b, c, d, \sigma, \phi)$ to the parameters in Eqs. (9)-(11); then we need to invert those equations to find the relative epicycle elements $\mathbf{x} = (\hat{a}, e, \hat{I}_0, \hat{\Omega}_0, \alpha_P, \alpha_e)$. Finally from these elements and the parameters describing the motion of the guiding centre, we can determine the absolute orbital elements required for each satellite.

We start by considering the relationship between the design parameters and the parameters in Eqs. (9)-(11). To this end we consider the equation of the projected ellipse in the $(\upsilon, \zeta)$ plane. This can be written as:

$$\left(\frac{(\upsilon - c)\cos\sigma + \zeta \sin\sigma}{a}\right)^2 + \left(\frac{-(\upsilon - c)\sin\sigma + \zeta\cos\sigma}{b}\right)^2 = 1 \tag{26}$$

or expanding out, in the form:

$$R(\upsilon - c)^2 + 2S(\upsilon - c)\zeta + T\zeta^2 = 1 \tag{27}$$

where

$$R = \left(\frac{\cos\sigma}{a}\right)^2 + \left(\frac{\sin\sigma}{b}\right)^2 \tag{28}$$

$$S = \sin\sigma\cos\sigma\left(\frac{1}{a^2} - \frac{1}{b^2}\right) \tag{29}$$

$$T = \left(\frac{\sin\sigma}{a}\right)^2 + \left(\frac{\cos\sigma}{b}\right)^2 \tag{30}$$

It is readily apparent that:

$$\upsilon_0 = c \tag{31}$$

as this is the offset along the $\upsilon$ axis. We can find the parameters $\upsilon_M$ and $\zeta_M$ from the fact these are the limiting values of the $\upsilon$ and $\zeta$ coordinates around the ellipse. These may be found from Eqs. (27) by differentiating with respect to either $\upsilon$ or with respect to $\zeta$ and setting the derivatives to vanish. It is straight-forward then to see that:

$$\upsilon_M^2 = \frac{T}{RT - S^2} \tag{32}$$

and

$$\zeta_M^2 = \frac{R}{RT - S^2} \tag{33}$$

It is also readily shown from Eqs. (28) to (30) that $RT - S^2 = 1/(ab)^2$ and hence:

$$\upsilon_M = \left(a^2\cos^2\sigma + b^2\sin^2\sigma\right)^{\frac{1}{2}} \tag{34}$$

$$\zeta_M = \left(a^2\sin^2\sigma + b^2\cos^2\sigma\right)^{\frac{1}{2}} \tag{35}$$

All that remains is to determine the phases $\phi_\upsilon$ and $\phi_\zeta$. To do this we need to consider the initial conditions. The value of $\tau$ is the time along the guiding centre motion and $\tau = 0$ corresponds to the moment the guiding centre crosses the equator at the ascending node. We may choose to arrange the formation at this time, but it may be more convenient to set the phases around the projected ellipse at some other time. We therefore suppose that the formation initial conditions are chosen at time $\tau_i$. If the initial value of $\zeta$ is $\zeta_i$ then

$$\sin(\tau_i + \phi_\zeta) = \frac{\zeta_i}{\zeta_M} \tag{36}$$

There are two possible phases satisfying this, which is resolved by the sign of $\dot{\zeta}_i$. Similarly, $\phi_\upsilon$ can be determined from Eqn (10) as follows:

$$\sin(\tau_i + \phi_\upsilon) = \frac{\upsilon_i - c}{\upsilon_M} \tag{37}$$

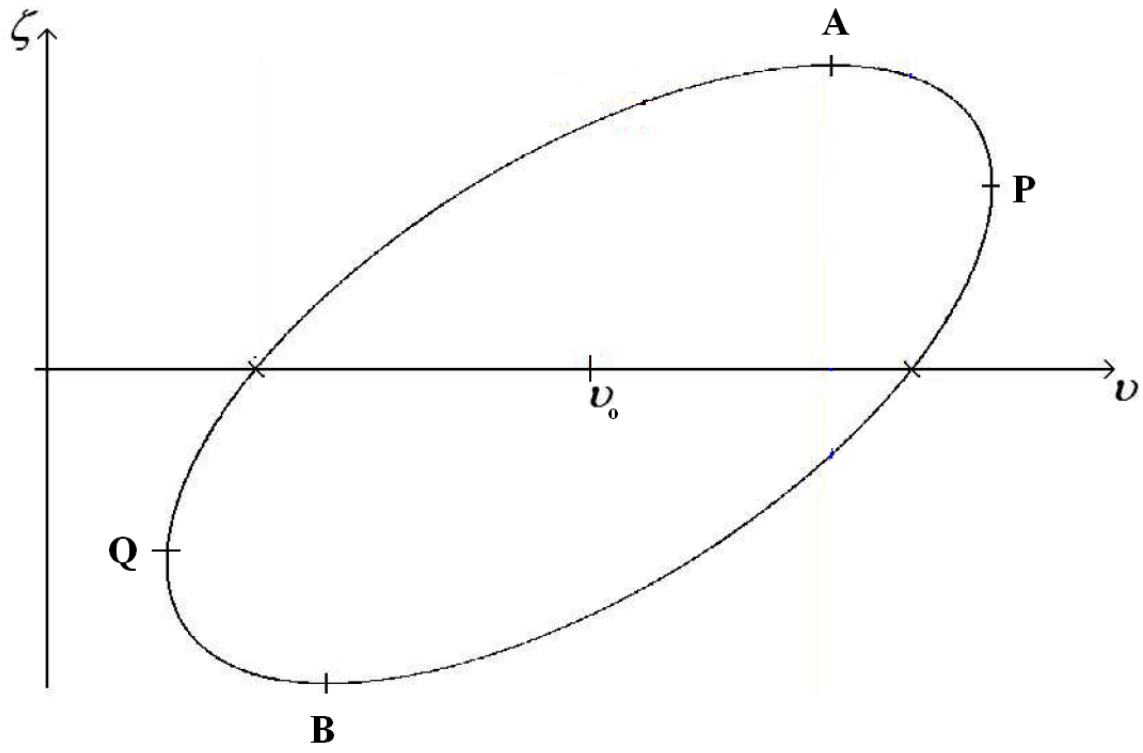


Figure 9: Intermediate parameters and key points on ellipse for calculating orbital parameters

To determine the signs of these derivatives we split the projected ellipse into four arcs divided by the points $A, B, P$ and $Q$, as shown in Fig. 9. At the points $A$ and $B$ $\zeta = \pm\zeta_M$ and at $P$ and $Q$ $\upsilon = \pm\upsilon_M$. The signs of the derivatives are given in Table 1, where the sign is related to the parameter $d$ determining whether the motion around the projected ellipse is clockwise or anticlockwise. The four points dividing the projected ellipse can be determined from the derivative:

$$\frac{d\zeta}{d\upsilon} = -\frac{R(\upsilon - c) + S\zeta}{S(\upsilon - c) + T\zeta} \tag{38}$$

and the numerator vanishes at $A$ and $B$ while the denominator vanishes at $P$ and $Q$. The signs of these expressions determine which of the four arcs the initial conditions lie in, as shown in Table 1.

Table 1: $\zeta$ phase at numbered ellipse points

| *Arc* | $\dot{\zeta}/\lvert\dot{\zeta}\rvert$ | $\dot{\upsilon}/\lvert\dot{\upsilon}\rvert$ | $R\upsilon + S\zeta$ | $S\upsilon + T\zeta$ |
|---|---|---|---|---|
| $QA$ | d | d | $< 0$ | $> 0$ |
| $AP$ | -d | d | $> 0$ | $> 0$ |
| $PB$ | -d | -d | $> 0$ | $< 0$ |
| $BQ$ | d | -d | $< 0$ | $< 0$ |

## 5.1 Internal Satellite Motions

In the previous section we inverted the design parameters to find the generic orbital parameters used in (9) -(11). As described earlier, our formations can be designed so that the pattern moves as a whole with respect to the guiding centre, or can be fixed with respect to the guiding centre. In this section we shall fix the internal motions of the individual satellites within the formation, but allow the formation to drift relative to the guiding centre. In this case we use expressions (13) - (15). Our purpose is to invert these expressions to find the individual satellite orbital elements: $(\widehat{I}_{k0}, \widehat{\Omega}_{k0}, \alpha_{Pk}, e_k, \widehat{a}_k, \alpha_e)$. As noted earlier, we can annul the differential secular drifts by fixing the relative semi-major axis of each satellite's orbit. In the case when only $J_2$ is considered this gives [15]:

$$\widehat{a}_k = -2aJ_2 \left(\frac{R}{a}\right)^2 \sin 2I\widehat{I}_{k0} \tag{39}$$

where $R$ is the equatorial Earth radius, and $a$ and $I$ are the orbital elements for the guiding centre. Of the other parameters we can obtain the following directly:

$$e_k = \frac{\upsilon_M}{2} \tag{40}$$

$$\alpha_{Pk} = -\phi_\upsilon \tag{41}$$

$$\widehat{I}_{k0} = \zeta_M \cos\phi_\zeta \tag{42}$$

From these results and equation (8) we obtain:

$$\widehat{\Omega}_{k0} = -\zeta_M \frac{\sin\phi_\zeta}{\sin I} - \widehat{\theta}_k\tau_i \tag{43}$$

The last term accounts for the relative secular shift around the equator if we fix initial conditions at some other latitude. This just leaves $\alpha_e$ to be determined, which is now

straight forward using Eq. (13) as all other terms are now known. This completes the inversion.

## 5.2 Using Complete Relative Motion

When we include the solid body motion then we need to invert Eqs. (19) - (23). In this case, from Eqs. (22) and (23) we can solve for $\widehat{I}_{k0}$ and $\widehat{\Omega}_{k0}$:

$$\widehat{I}_{k0} = \zeta_M \cos\phi_\zeta + \frac{3}{4} J_2 \left(\frac{R}{a}\right)^2 \sin 2I \tag{44}$$

and

$$\widehat{\Omega}_{k0} = \zeta_M \frac{\sin\phi_\upsilon}{\sin I} - \widehat{\theta}_k \tau_i \tag{45}$$

We next use Eqs. (20) and (21) to solve for $e_k$ and $\alpha_{Pk}$. To see how this is done we introduce the variable $y = e_k \sin(\alpha_{Pk} + \kappa\tau_i)$. These equations can then be written as:

$$(e_k^2 - y^2)\tan^2\phi_\zeta = (\chi - y)^2 \tag{46}$$

and

$$\frac{1}{4}\upsilon_M^2 - \chi^2 = e_k^2 + 2\chi y \tag{47}$$

We can eliminate the linear term in $y$ between these to obtain:

$$e_k^2 - y^2 = \frac{1}{4}\upsilon_M^2 \cos^2\phi_\zeta \tag{48}$$

Substituting this back into Eqs. (20) and (21) then results in:

$$e_k^2 = \chi^2 + \left(\frac{1}{2}\upsilon_M\right)^2 - \chi\upsilon_M \sin\phi_\upsilon \tag{49}$$

and

$$\tan(\alpha_{Pk} + \kappa\tau_i) = \frac{\chi - \frac{1}{2}\upsilon_M \sin\phi_\zeta}{\frac{1}{2}\upsilon_M \cos\phi_\zeta} \tag{50}$$

Finally $\alpha_e$ can be found from Eq. (19) as everything else is now known.

Table 2: Formation design parameters for six-satellite varying radius projected circle formation.

| *Satellite* | *a (km)* | *b (km)* | *c (km)* | *d* | $\sigma$ *(deg)* | $\varphi$ *(deg)* |
|---|---|---|---|---|---|---|
| 1 | 10.000 | 2.000 | 0.000 | 1 | 45.0 | 42.0 |
| 2 | 10.000 | 2.000 | 0.000 | 1 | 45.0 | 222.0 |
| 3 | 10.000 | 2.000 | 0.000 | 1 | 105.0 | 102.0 |
| 4 | 10.000 | 2.000 | 0.000 | 1 | 105.0 | 282.0 |
| 5 | 10.000 | 2.000 | 0.000 | 1 | 165.0 | 162.0 |
| 6 | 10.000 | 2.000 | 0.000 | 1 | 165.0 | 342.0 |

Table 3: Generalised elliptic motion parameters for six-satellite varying radius projected circle formation.

| *Satellite* | $\upsilon_M$ *(km)* | $\zeta_M$ *(km)* | $\phi_\upsilon$ *(deg)* | $\phi_\zeta$ *(deg)* |
|---|---|---|---|---|
| 1 | 7.211 | 7.211 | 93.37 | 115.99 |
| 2 | 7.211 | 7.211 | -86.63 | -64.01 |
| 3 | 3.230 | 9.673 | -38.58 | 101.61 |
| 4 | 3.230 | 9.673 | 141.42 | -78.38 |
| 5 | 9.673 | 3.230 | -72.25 | 67.95 |
| 6 | 9.673 | 3.230 | 107.75 | -112.05 |

# 6 The Design Process

We now demonstrate the design process and computation of the orbital elements for individual satellites. This will then enable us to evaluate the accuracy of this methodology by propagating the resulting orbits forward and projecting onto the sky. For illustration we have chosen to consider the varying radius projected circle formation shown in Fig. 7. The formation design parameters for this are given in Table 2.

The first stage is to determine the parameters in Eqs. (9)-(11) for these satellites. $\upsilon_0 = 0$ for all the satellites, and the remaining parameters are given in Table 3.

These parameters are next converted into relative epicycle parameters using either internal satellite motions, as in Eqs. (5) - (8), or also incorporating the solid body motion of the formation about the guiding centre described by Eqs. (2) - (4). We show both sets of orbital parameters in Tables 4 and 5 respectively. These orbital parameters have been calculated based upon a guiding centre reference orbit with inclination of 45

Table 4: Relative epicycle parameters for six-satellite varying radius projected circle formation using internal satellite motions only.

| *Satellite* | $\widehat{a}_k$ *(m)* | $\widehat{I}_k$ *(deg)* | $\widehat{\Omega}_k$ *(deg)* | $e_k$ | $\alpha_{Pk}$ *(deg)* | $\alpha_e$ *(deg)* |
|---|---|---|---|---|---|---|
| 1 | 5.6813 | -0.0259 | -0.0750 | 0.000515 | -93.3737 | -0.1121 |
| 2 | -5.6813 | 0.0259 | 0.0750 | 0.000515 | 86.6263 | 0.1121 |
| 3 | 3.5013 | -0.0159 | -0.1097 | 0.000231 | 38.5784 | -0.0612 |
| 4 | -3.5013 | 0.0159 | 0.1097 | 0.000231 | -141.4216 | 0.0611 |
| 5 | -2.1800 | 0.0099 | -0.0346 | 0.000691 | 72.2489 | 0.0510 |
| 6 | 2.1800 | -0.0099 | 0.0346 | 0.000691 | -107.7511 | -0.0509 |

Table 5: Relative epicycle parameters for six-satellite varying radius projected circle formation using complete relative motions.

| *Satellite* | $\widehat{a}_k$ *(m)* | $\widehat{I}_k$ *(deg)* | $\widehat{\Omega}_k$ *(deg)* | $e_k$ | $\alpha_{Pk}$ *(deg)* | $\alpha_e$ *(deg)* |
|---|---|---|---|---|---|---|
| 1 | -2.8014 | 0.0128 | -0.0750 | 0.001268 | -91.3698 | -0.1119 |
| 2 | -14.1639 | 0.0645 | 0.0750 | 0.000241 | -82.7803 | 0.1118 |
| 3 | -4.9814 | 0.0227 | -0.1097 | 0.000636 | -73.5198 | -0.0610 |
| 4 | -11.9839 | 0.0546 | 0.1097 | 0.000915 | -101.3640 | 0.0610 |
| 5 | -10.6627 | 0.0485 | -0.0346 | 0.000231 | -24.3689 | 0.0508 |
| 6 | -6.3027 | 0.0287 | 0.0346 | 0.001427 | 261.5117 | -0.0509 |

degrees, semi-major axis of 7000km and right ascension of ascending node of 0 degrees.

These relative orbital parameters can now either be converted into absolute epicycle orbit parameters or propagated using the analytic epicycle orbit propagator described in [15]. The along-track and cross-track relative coordinates $\upsilon$ and $\zeta$ were then found using an exact transformation from the absolute epicycle coordinates to remove the guiding centre location. We start by considering the case when both the internal and solid body motions are incorporated into the dynamical model. Propagating the six orbits for one day we obtain the projected paths on the sky shown in Fig. 10. This shows that the pattern is well maintained but each of the ellipses precesses slightly in the sky and this will lead to some distortion of the pattern. This arises from a small frequency mismatch between the $J_3$ terms and the eccentricity terms. It is, of course, envisaged that any such formation would have active control to damp such drifts in formation geometry, but this shows that the level of required control is small as the

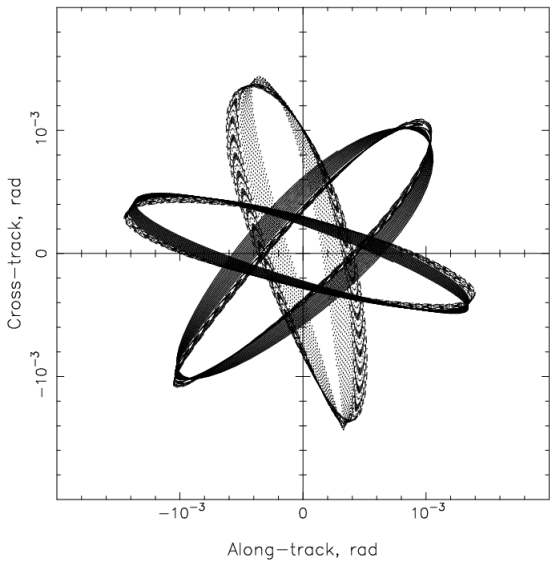


Figure 10: Relative orbit paths for satellite formation designed using complete relative motions.

drift is much smaller than the size of the formation itself.

We can quantify the growth in errors over this propagation by comparing the propagated positions of the satellites with their locations in the ideal model used here. We show the variation of this positional error in Fig. 11 which shows that if unchecked, the position error grows to 2km in one day. This is an upper estimate of the error as the ellipses precess in the same sense in the plane of the sky, and so the relative errors in the geometry will be smaller.

Next we consider the same formation geometry when we only consider the internal motions and allow the formation to drift with respect to the guiding centre. We show the same propagation in this case in Fig. 12. This shows a more severe distortion from the expected geometry. This arises because we need to remove the guiding centre motion in the sky. This guiding centre motion may be modelled by propagating an orbit where the relative epicycle parameters are zero (i.e. an orbit similar to that of the guiding centre but where periodic terms are also retained). Subtracting this motion from the motions of each of the six satellites shows a more regular pattern, as shown in

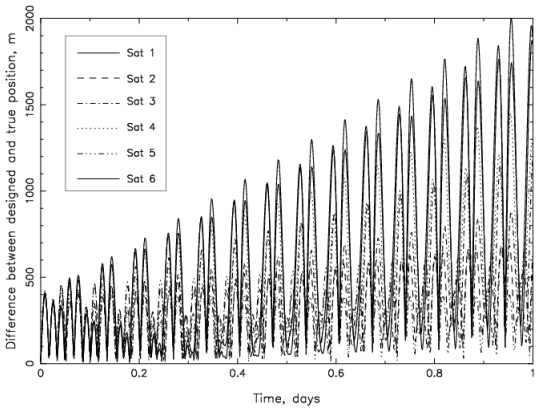


Figure 11: Distance between satellite true position and ideal position for satellite formation designed using complete relative motions.

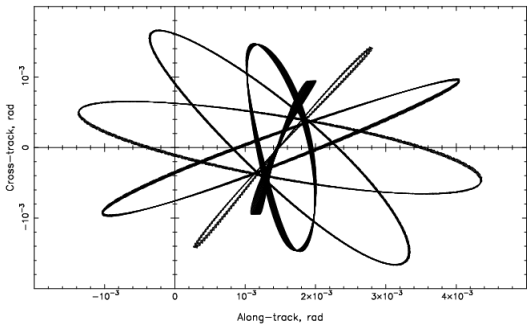


Figure 12: Relative orbit paths for satellite formation designed using internal satellite motions only.

Fig. 13. We note that the origin in this figure is no longer the guiding centre but is the centre of the formation. We can clearly see that the desired configuration of satellites has been achieved.

This figure shows that less control is required to maintain the formation geometry. We may quantify this by propagating the difference between ideal location and the propagated location of each of the six satellites. This is shown in Fig. 14

The desired position is calculated on the assumption that each satellite remains on the design ellipse path, moving with an orbital period equal to the guiding centre orbital period. This deviation is periodic, depending upon position on the ellipse, and for the satellite with the largest deviation, grows to approximately 900m in one day.

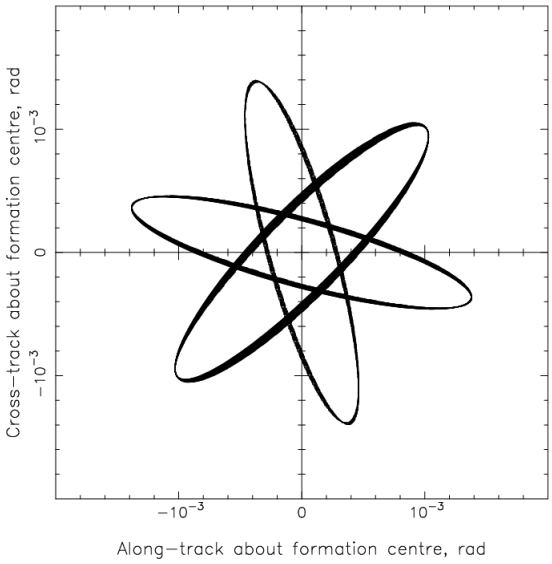


Figure 13: Relative orbit paths once formation centre motion has been subtracted.

This deviation is not an error but simply a result of the real dynamics when no control is applied. The position error is reduced by 45% when the pattern is allowed to oscillate with respect to the guiding centre.

# 7 Conclusion

In this paper we have exploited an analytic model for the relative motion of satellites in near circular low earth orbit orbits. This model conveniently separates the relative motion into a moving guiding centre, which absorbs all the principal secular drift terms and periodic motion of satellites with respect to this guiding centre. The periodic motion itself is further conveniently split between a rigid body motion of the formation about the guiding centre and individual satellite motions that change the geometry of the formation.

The analytic model gives a very simple description of the motions of these satellites projected onto the plane of the sky. The motion is described by a tilted ellipse. The parameters of these projected ellipses are directly related to the orbital elements of the satellites. A significant aspect of this analytic model is that these expressions can

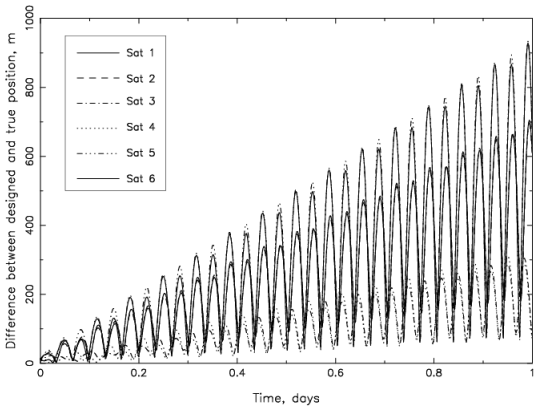


Figure 14: Distance between satellite true position and ideal position for satellite formation designed using internal satellite motions only

be inverted, and hence we can design satellite low earth orbit formations based upon their projected geometry and then invert to determine what orbital parameters we require for each satellite. This makes for a powerful design tool for low earth orbit constellations.

We have shown that a number of interesting geometries for low earth orbit formations can be established, in which a series of fixed baselines can be maintained, or pulsating formations where the baseline varies periodically around the orbit. We have evaluated the formation geometry with direct simulation of the satellite orbits to show the rate of departure from the idealised geometry. This provides an indication of the level of orbital control that would be needed to maintain the formation geometry. While this has not been formally evaluated using a control methodology, because we are exploiting the natural $J_2$ and $J_3$ dynamics of the geopotential, the control required is very affordable even for small satellites with limited propellant capacity. We have demonstrated for one pulsating geometry that a 45% saving in propellant can be achieved if we allow the formation geometry to float with respect to the guiding centre, while maintaining the geometry of the formation.

## Acknowledgements

The authors would like to acknowledge the support of the UK Engineering & Physical Sciences Research council who sponsored this research.

# References

[1] B. D. Tapley, S. Bettadpur, M. Watkins, and C. Reigber. The gravity recovery and climate experiment: Mission overview and early results. *Geophys. Res. Lett.*, 31(9), May 2004. L09607.

[2] K. Stewart A. Hernandez-Pellerano D. Speer, G. Jackson. The space technology 5 avionics system. In *Aerospace Conference, IEEE Proceedings*, March 2005.

[3] J.A. Slavin C.C. Carlisle, E.H. Webb. Space technology 5 - changing the mission design without changing the hardware. In *Aerospace Conference, IEEE Proceedings*, pages 758–767, Big Sky, Montana, March 2005. 10.1109/AERO.2005.1559368.

[4] M. E. Hametz, D. J. Conway, and K. Richon. Design of a formation of earth orbiting satellites: The auroral lites mission. In *Proceedings of the 1999 NASA/GSFC Flight Mechanics Symposium*, pages 295–308, Greenbelt. Maryland, 1999.

[5] H. Fiedler I. Hajnsek-M. Werner M. Younis M. Zink G. Krieger, A. Moreira. Tandem-x: A satellite formation for high-resolution sar interferometry. *IEEE Transactions on Geoscience and Remote Sensing*, November 2007.

[6] E. Gill and H. Runge. Tight formation flying for an along-track sar interferometer. *Acta Astronautica*, 55(3–9):473–485, 2004.

[7] A. Moccia, S. Vetrella, and R. Bertoni. Mission analysis and design of a bistatic synthetic aperture radar on board a small satellite. *Acta Astronautica*, 47(11):819–829, 2000.

[8] G. Krieger M. Zink and T. Amiot. Interferometric performance of a cartwheel constellation for terrasar-l. In *Proceedings of FRINGE Workshop 2003*, volume 550 of *ESA Special Publication*, Frascati, Italy, December 2003.

[9] W.H. Clohessy and R.S. Wiltshire. Terminal guidance system for satellite rendezvous. *Journal of the Aerospace Sciences*, 27(9):653–658, 674, 1960.

[10] Y. Hashida and P. Palmer. Epicyclic motion of satellites about an oblate planet. *Journal of Guidance, Control and Dynamics*, 24(3):586–596, 2001.

[11] C. Sabol, R. Burns, and C. A. McLaughlin. Satellite formation flying design and evolution. *Journal of Spacecraft and Rockets*, 38(2):270–278, 2001.

[12] Christopher Lane and Penina Axelrad. Formation design in eccentric orbits using linearized equations of relative motion. *Journal of Guidance, Control and Dynamics*, 29(1):146–160, 2006.

[13] V. M. Guibout and D. J. Scheeres. Spacecraft formation dynamics and design. *Journal of Guidance, Control and Dynamics*, 29(1):121–133, 2006.

[14] M. Halsall and P. L. Palmer. An analytic relative orbit model incorporating $j_3$. In *AIAA/AAS Astrodynamics Specialist Conference and Exhibit*, Keystone, Colorado, 2006. AIAA-2006-6761.

[15] M. Halsall and P. L. Palmer. Modelling natural formations of leo satellites. *Journal of Celestial Mechanics and Dynamical Astronomy*, 99:105–127, 2007.

[16] Y. Hashida and P. Palmer. Epicyclic motion of satellites under rotating potential. *Journal of Guidance, Control and Dynamics*, 25(3):571–581, 2002.

[17] D. Adamo. A meaningful relative coordinate systemfor generic use. In *AIAA/AAS Astrodynamics Specialist Conference*, Lake Tahoe, California, 2005. AAS 05-306.